

# Digital Animation of Powder-Snow Avalanches

## Supplemental Material

FILIPE NASCIMENTO, ICMC-USP, Brazil

FABRICIO S. SOUSA, ICMC-USP, Brazil

AFONSO PAIVA, ICMC-USP, Brazil

### 1 ABLATION STUDY

This section explores the influence of the model's parameters on the resulting simulation. All simulations are performed in 2D and consider the powder-snow avalanche (PSA) triggered by the detachment of a body of snow cover at rest,  $\bar{u} = 0$ , defined by a release area in a flat ramp with  $25^\circ$  slope discretized by a PSL mesh with 20K cells. Unless otherwise specified, the simulations presented in this section use the set of parameter values listed in Table 1. Moreover, in the PSL algorithm, we set the maximum number of iterations as  $n_{\text{piso}} = n_{\text{corr}} = 2$  and CFL condition with a maximum Courant number of  $Co_{\max} = 0.2$ .

Table 1. Model parameters values.

layer	parameter	description	value
DSL	$\hat{\rho}_s$	snow density [ $kg/m^3$ ]	500
	$v$	Voellmy's dry friction	0.155
	$\xi$	Voellmy's dynamic friction [ $m/s^2$ ]	5000
	$E_b$	specific erosion energy	50
TL	$\gamma_\alpha$	mass injection factor	0.1
	$\gamma_u$	velocity injection factor	1.6
	$L_{\text{front}}$	avalanche front size[m]	40
PSL	$\hat{\rho}_a$	air density [ $kg/m^3$ ]	1.2
	$\hat{\mu}_a$	air viscosity [ $m^2/s$ ]	$1.4 \times 10^{-5}$
	$\hat{\rho}_s$	powder-snow density [ $kg/m^3$ ]	1.4
	$\hat{\mu}_s$	powder-snow viscosity [ $m^2/s$ ]	$10^{-4}$
	$\Gamma$	diffusion coefficient	$2 \times 10^{-4}$

The **powder-snow density**  $\hat{\rho}_s$  plays a central role in the motion of the powder cloud. From the momentum equation of the PSL model, the density field's gradient scales gravity's action. Higher density differences induce higher accelerations and increase the velocity while carrying more inertia. Moreover, high-density volumes have stronger momentum and may displace more surrounding fluid. The following experiment lists avalanches with powder-snow densities varying from near-air density to higher values. The figure shows a powder-snow avalanche sliding down a flat ramp at the instant  $t = 50$ s for four density values  $\hat{\rho}_s \in \{1.4, 2.5, 5.0, 7.0\}$ . Note how the cloud distribution concentrates towards the head of the PSL as the density value increases and how lower densities lead to amplifying the Kelvin-Helmholtz instabilities.

Authors' addresses: Filipe Nascimento, filipedecn@gmail.com, ICMC-USP, São Carlos, SP, Brazil; Fabricio S. Sousa, fsimeoni@icmc.usp.br, ICMC-USP, São Carlos, SP, Brazil; Afonso Paiva, apneto@icmc.usp.br, ICMC-USP, São Carlos, SP, Brazil.

In the DSL model, the **erosion energy**  $E_b$  modulates the entrainment rate. Higher values lead to lower entrainment rates. The erosion energy value represents the energy required to detach mass from the snow cover. The entrainment process maintains the avalanche motion by introducing mass into the body, increasing the momentum. Therefore, higher entrainment rates contribute to the acceleration of the avalanche. Figure shows the resulting PSAs using erosion energy values  $E_b \in \{15, 25, 100, 400\}$ .

Regarding the TL, the injection of mass and velocity into the PSL contains some parametrization that dictates the final shape of the cloud. The parameters considered are:

- **Mass Injection Factor**  $\gamma_\alpha$  controls the percentage of entrained mass by the DSL into the PSL. Figure 3 shows the powder clouds produced with four values of  $\gamma_\alpha \in \{0.01, 0.1, 0.4, 0.9\}$ . The highest values accumulate in the front, where injection occurs, and flow in distinct patterns. Lower values of  $\gamma_\alpha$  produce visible structures, while higher values smooth out and fill the cloud volume. Such differences result from the diffusion process driven by the gradient of the powder-snow concentration  $\alpha$ , as greater gradient values induce higher diffusion rates.
- **Velocity Injection Factor**  $\gamma_u$  scales the combined effect of air intake and snowpack ejection displacement translated into velocity surges. Figure 4 shows the powder clouds produced with four values of  $\gamma_u \in \{1, 2, 4, 8\}$ . The injection velocity has an apparent effect on the size of the cloud. Higher velocities lead to higher plumes and turbulent motion.
- **Avalanche front size**  $L_{\text{front}}$  controls the length of the avalanche front, i.e., the region where  $\gamma_\alpha$  and  $\gamma_u$  have a more significant effect. Figure 5 shows the powder clouds produced with four values of  $L_{\text{front}} \in \{10, 20, 40, 80\}$ . Smaller front regions result in short injection times from the same terrain location, leading to smaller plume heights. Also, separate plumes become more evident away from the front in such cases due to the spatial noise distribution in the terrain. Extensive front regions inject mass from the same terrain position longer, giving enough time to mix. Additionally, the overall height of the cloud increases as the injection velocities act longer.

## 2 MESH INDEPENDENCE STUDY

This study ensures that the solution is independent of the mesh resolution to determine the appropriate resolution for accurate results, i.e., the solution is invariant under mesh refinement. The experiments presented in this section utilize a 2D flat ramp with a  $25^\circ$  slope up to 1 km long. For instance, natural terrains can present avalanche runout distances of many kilometers. Such large scales inevitably bring computational challenges to numerical methods since the accuracy of the results depends directly on the mesh resolution.

Typical fluid simulations use grids with a cell size  $\delta x$  of a few centimeters wide, if not smaller. However, compared to avalanche sizes, such resolutions can quickly increase the number of cells to hundreds of millions. Therefore, cells in the order of meters become necessary. The following experiments explore the convergence of the PSL model given a set of PSL meshes with 375K ( $\delta x = 0.1$ ), 75K ( $\delta x = 0.5$ ), 38K ( $\delta x = 1.0$ ), 8K ( $\delta x = 5.0$ ), and 4K ( $\delta x = 10.0$ ) faces.

Figure 6 depicts a series of PSAs using different mesh resolutions. As the cell size  $\delta x$  increases, the higher numerical diffusivity becomes apparent, leading to fewer flow details. For a qualitative view, the snow volume fraction field for the simulations with  $\delta x = 0.1$  and  $\delta x = 0.5$  are similar, indicating the solution's convergence. Figure 7 shows the boxplots for the distribution of the Courant numbers,  $Co = (\|\dot{\mathbf{u}}\|_2 \delta t) / \delta x$ , and the time-steps managed with CFL condition for each mesh resolution.

### 3 ACCURACY OF THE INTERPOLATION SCHEMES

This experiment shows the effects caused by the order of accuracy of the interpolation schemes utilized in the convective terms from the PSL. Figure 8 shows a PSA simulation in a flat ramp with  $25^\circ$  slope discretized by a PSL mesh with 86K cells using van Leer's TVD (2nd order) and upwind (1st order) schemes. As can be seen, the upwind scheme produces a numerical diffusion that smears off the sharp interface between the powder-snow cloud and ambient air. On the other hand, the TVD scheme is robust to numerical diffusion with a computational cost similar to the upwind scheme.

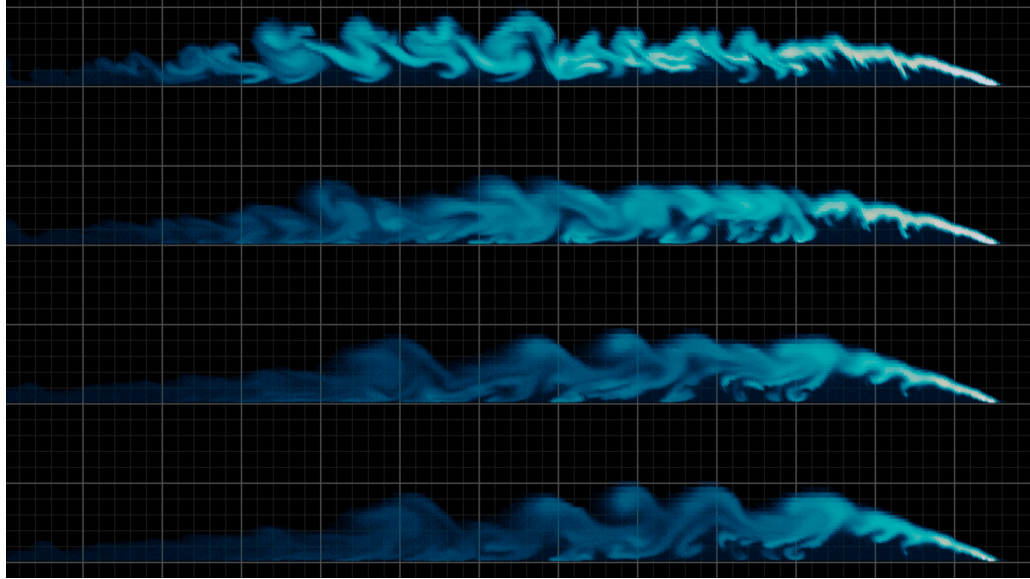


Fig. 1. Resulting PSAs at  $t = 50\text{s}$  with four distinct values for the powder-snow density  $\hat{\rho}_s \in \{1.4, 2.5, 5.0, 7.0\}$ , from top to bottom, respectively. Brighter colors represent higher values of the powder-snow concentration  $\alpha$ .

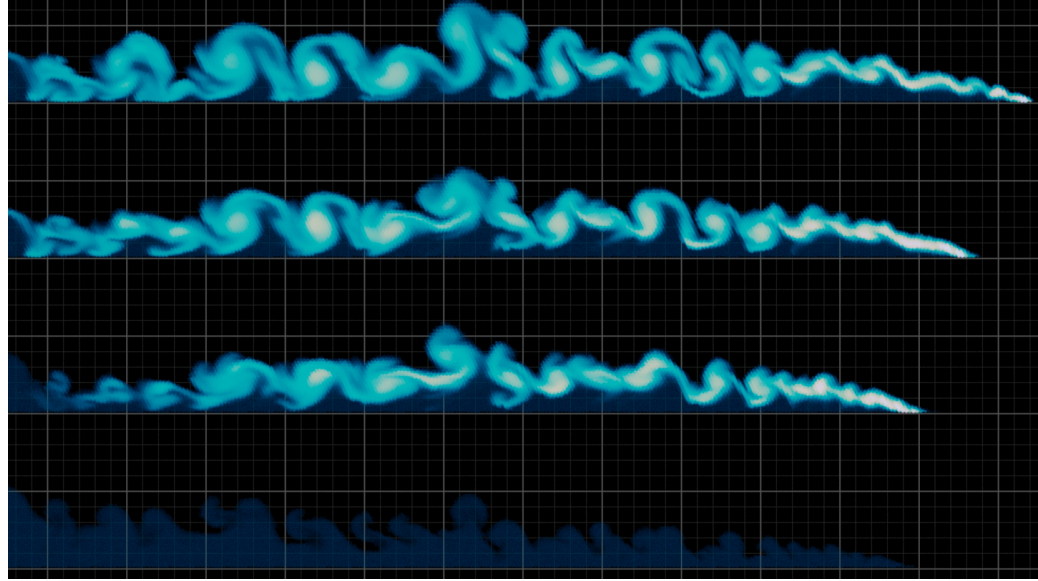


Fig. 2. Resulting PSAs at  $t = 30s$  with four distinct values for the erosion energy  $E_b \in \{15, 25, 100, 400\}$ , from top to bottom, respectively. Brighter colors represent higher values of the powder-snow concentration  $\alpha$ .

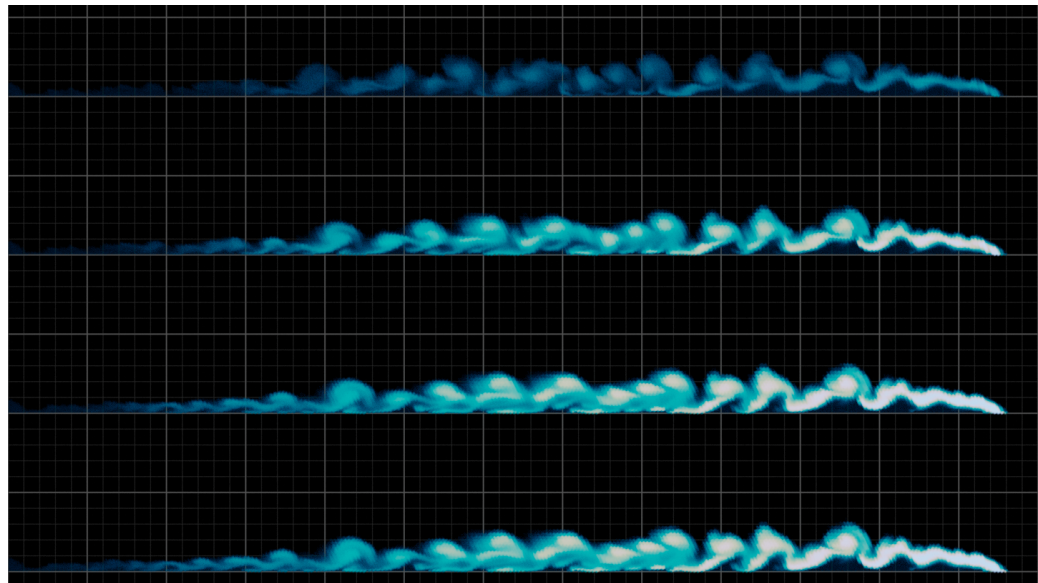


Fig. 3. Resulting PSAs at  $t = 50s$  with four distinct values for the mass injection factor  $\gamma_\alpha \in \{0.01, 0.1, 0.4, 0.9\}$ , from top to bottom, respectively. Brighter colors represent higher values of the powder-snow concentration  $\alpha$ .

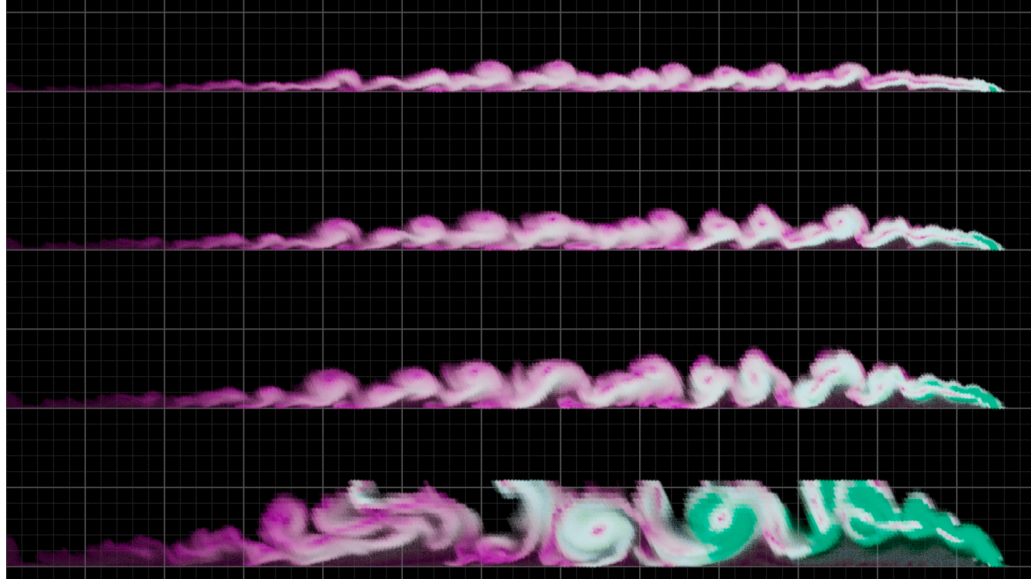


Fig. 4. Resulting PSAs at  $t = 50$ s with four distinct values for the velocity injection factor  $\gamma_u \in \{1, 2, 4, 8\}$ , from top to bottom, respectively. The colors represent low (magenta) and high velocities (green).

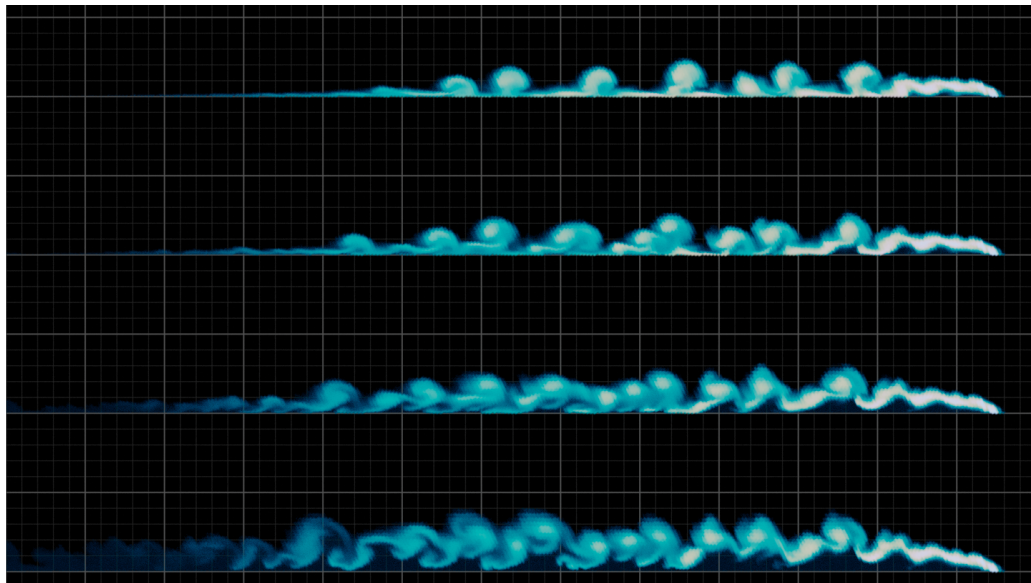


Fig. 5. Resulting PSAs at  $t = 50$ s with four distinct values for the size of the avalanche front  $L_{\text{front}} \in \{10, 20, 40, 80\}$ , from top to bottom, respectively. Brighter colors represent higher values of the powder-snow concentration  $\alpha$ .

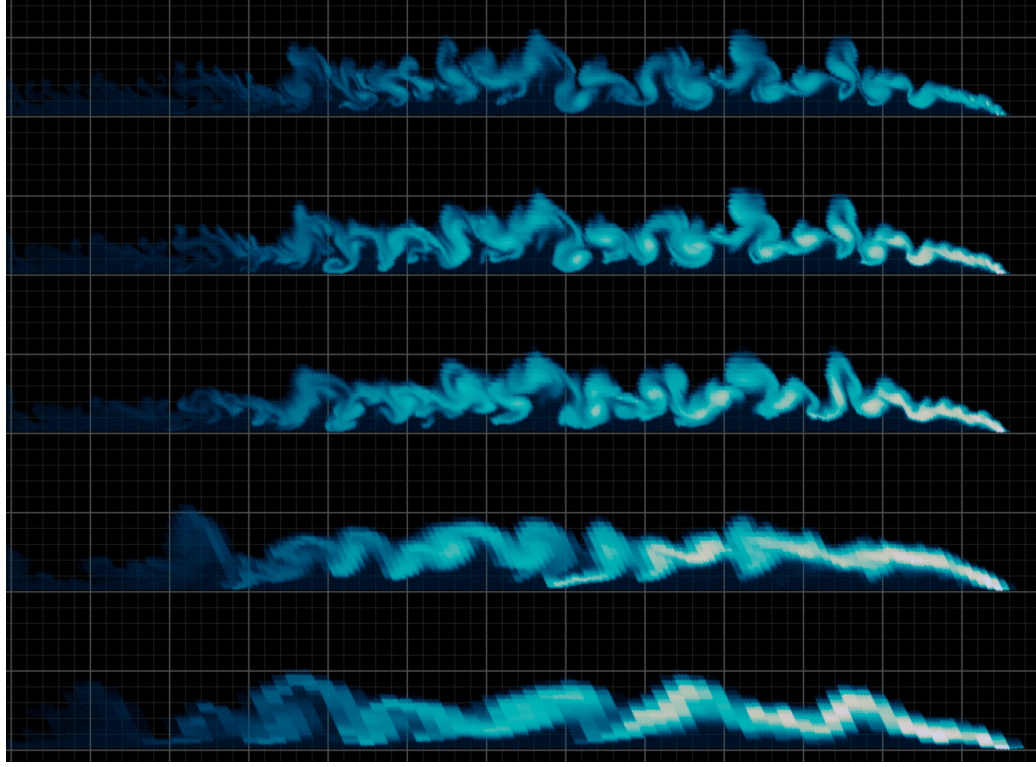


Fig. 6. PSA simulations generated using the same parameters and initial conditions for different mesh resolutions. From top to bottom, PSL meshes with cell sizes  $\delta x \in \{0.1, 0.5, 1.0, 5.0, 10.0\}$ . Note how the cloud details, such as vortices and curved shapes, vanish as the cell size increases. Brighter colors represent higher values of the powder-snow concentration  $\alpha$ .

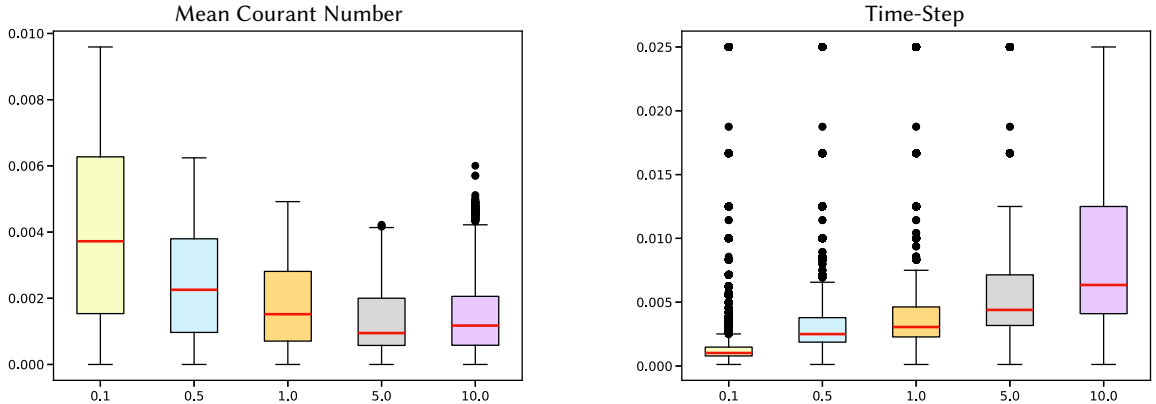


Fig. 7. The variation in the mean Courant values (left) and adaptive time-steps (right) registered in the different mesh resolutions with cell sizes  $\delta x \in \{0.1, 0.5, 1.0, 5.0, 10.0\}$  (x-axis in the boxplots). As expected, coarse grids lead to smaller Courant numbers and allow larger time-steps.

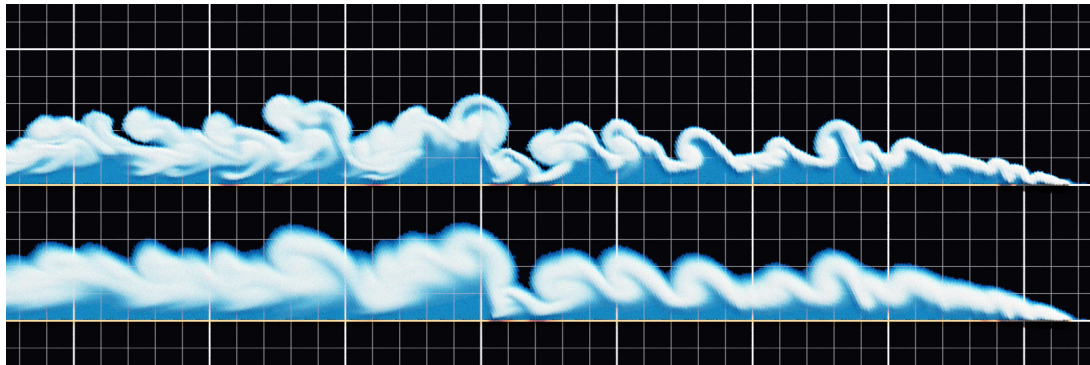


Fig. 8. PSA simulations using TVD (*top*) and upwind (*bottom*) interpolation schemes at  $t = 30$ s. The color encodes the powder-snow concentration  $\alpha$  varying from low (white) to high (blue) values.